ROYAL SOCIETY OF CHEMISTRY

Check for updates

Tetrazole derivatives synthesis *via* green one-pot oxidation of benzyl alcohol using Cu(II) immobilized on nanodiamond@folic acid catalyst

Arezoo Ramezani, Reza Ghalavand, Zahra Nasri [iD] and Hossein Ghafuri [iD] *

Tetrazoles are highly significant in pharmaceuticals, drug delivery, and anticancer treatments. In this work, the development of a highly effective nanocatalyst, which was synthesized by functionalizing nanodiamonds (NDs) substrate with folic acid (FA) and stabilizing Cu(II) on the nanocomposite. The ND@FA-Cu(II) nanocatalyst has demonstrated superior thermal stability, non-toxicity, little catalyst consumption, and reusability (up to five cycles), rendering it both cost-effective and environmentally sustainable. The catalytic efficacy of ND@FA-Cu(II) was assessed in the production of 1H-tetrazole derivatives employing two methodologies. A one-pot synthesis using malononitrile, sodium azide, and benzyl alcohol (oxidized in acetonitrile) effectively yielded 5-substituted 1H-tetrazoles. The second strategy involved the synthesis of 1H-tetrazoles from benzaldehyde, malononitrile, and sodium azide in ethanol under mild conditions *via* Knoevenagel condensation and 1,3-dipolar cycloaddition. This one-pot multicomponent reaction (MCR) minimizes by-products, enhances yields, and reduces reaction durations and solvent usage, providing a sustainable technique for tetrazole synthesis with 97% yield.

1 Introduction

Nanodiamonds (NDs) have garnered considerable interest in recent years owing to their extensive applications across multiple domains.[1–3] These nanoparticles are employed in applications including metal electroplating, medication administration, medical imaging, and the fabrication of metal and polymer matrix composites.[4,5] A primary benefit of nanodiamonds is their biocompatibility, as they demonstrate no adverse effects on live cells and are inherently non-toxic.[4,6] Their distinctive characteristics, including as elevated thermal conductivity, a chemically reactive surface, and a spherical morphology with an extensive surface area, provide them optimal candidates for the advancement of sophisticated nanocomposite coatings.[6,7]

Compared to other nanoparticles, nanodiamonds exhibit a highly adaptable surface chemistry that facilitates the modification of both chemical and physical properties, thus improving their stability and environmental compatibility.[8,9] This adaptable surface chemistry is essential for their function as catalysts.[10] The existence of many functional groups, including ketones, carboxyl, hydroxyl, and others, on the surface of nanodiamonds enhances their potential applications.[11,12] Research indicates that extending the heat oxidation duration enhances the quantity of carboxyl groups on the

nanodiamond surface, so converting them into highly efficient surface adsorbents and markedly augmenting their overall characteristics.

In recent developments, researchers have emphasized the importance of using surface-engineered supports such as mesoporous materials or graphene derivatives in catalytic systems to increase surface area, improve dispersion of active species, and enable catalyst recyclability.[13,14] Incorporating magnetically separable nanocomposites or green supports like ND can simultaneously address issues of catalyst recovery and environmental safety.[14]

Folic acid, a water-soluble form of vitamin B9, is characterized by its colorless and odorless nature, often presenting an orange-yellow hue.[15,16] This essential vitamin offers numerous advantages, including accessibility, affordability, and ease of use.[17] Its stability in alkaline environments exceeds that in acidic conditions,[18] with factors such as temperature, oxygen, light, and pH exerting significant influences on its stability. Since the human body cannot synthesize folic acid, dietary intake remains the primary source of this vital nutrient.[19] Comprising a pteridine ring attached to *p*-amino benzoic acid and glutamic acid, folic acid is a member of the vitamin B complex. This small, water soluble molecule exhibits high stability.[20] And functions as an enzymatic cofactor, playing a crucial role in methyl group transfer reactions and various biological functions. Current research highlights folic acid's versatility and potential applications, particularly its role as a green linker facilitating the anchoring of metals on NDs.

Catalysts and Organic Synthesis Research Laboratory, Department of Chemistry, Iran University of Science and Technology, Tehran 16846-13114, Iran. E-mail: ghafuri@iust.ac.ir; Fax: +98-21-77491204; Tel: +98-21-77240516-7

Functionalizing supports with organic acids or macrocyclic ligands such as folic acid or phthalocyanines has proven effective in enhancing catalytic performance, improving metal anchoring, and promoting eco-friendly reaction conditions.[13]

Tetrazoles, nitrogen-containing heterocycles with electron-rich aromatic structures, are essential components in numerous active medicinal compounds.[21,22] This attribute renders the synthesis of tetrazoles especially vital in the development of novel medicines. These compounds demonstrate a variety of distinctive features, resulting in their widespread use in medicinal chemistry, drug delivery, anticancer therapy, and agriculture.[23,24] Tetrazole derivatives additionally function as precursors and protective agents in nanomaterial production. The extensive applicability and intriguing characteristics of tetrazoles have generated considerable interest in the creation of innovative synthesis methods.[25] Among the various reported methods for tetrazole construction, multicomponent reactions (MCRs) under mild, solvent-free, or green solvent conditions have gained much attention due to their efficiency, atom economy, and ability to generate diverse products in a single operation.[14,26] In recent years, significant breakthroughs have occurred in this field, and we have aimed to leverage these developments by utilizing cutting-edge methodologies to enhance tetrazole synthesis and optimize the effectiveness of the resultant molecules.

It is hypothesized that the Cu(II) in the synthesized ND@FA-Cu(II) nanocatalyst, as a Lewis acid with empty orbitals, can form dative (coordinate) bonds with the lone electron pairs on the oxygen atom of benzaldehyde and the nitrogen atom of malononitrile. This contact is predicted to activate the reactants on the catalyst surface, leading to the dipolar 1,3-cycloaddition process and subsequent production of the tetrazole. In light of these advances, this study introduces a novel heterogeneous nanocatalyst, ND@FA-Cu(II), synthesized *via* surface oxidation of nanodiamonds, covalent anchoring of folic acid, and coordination of Cu(II) ions. The designed system combines green materials, low catalyst loading, operational simplicity, and high catalytic performance. Notably, it enables the one-pot synthesis of a broad range of tetrazole derivatives in ethanol with excellent yields of up to 97% under mild and eco-friendly conditions. The catalyst exhibits high thermal stability and biocompatibility. It can be reused up to five cycles without significant efficiency loss. These features are confirmed by FT-IR, EDS, XRD, FE-SEM, and TGA analyses. Moreover, the ability to synthesize several novel tetrazole derivatives using a sustainable, green, and scalable protocol clearly distinguishes this system from previously reported methods, offering a practical platform for tetrazole synthesis in environmentally conscious synthetic chemistry.

2 Experimental

2.1. General

All solvents, chemicals, and reagents were purchased from Merck and Sigma-Aldrich. The spherical detonation NDs were obtained from Plasma Chem Company (Germany).

2.2. Preparation of ND@FA-Cu(II) nanocatalyst

To carboxylate nanodiamonds, 0.5 g of diamond nanoparticles were placed in the oven at a temperature of 450 °C for 5 h at a rate of 1°C min^{-1}.[27] In a round-bottomed flask (25 mL), 0.30 g of oxidized nanodiamond was mixed with 0.310 g of N, N′-dicyclohexylcarbodiimide (DCC), and 0.40 g of N-Hydroxysuccinimide (NHS) with 10 mL of DMSO. Then, to activate the carboxylic acid groups, it was stirred for 24 h at room temperature. In the next step, 0.265 g of folic acid was added to the above mixture, and it was stirred at room temperature for 8 h. Finally, the prepared nanoparticle was filtered and washed several times with DMSO and then ethanol. It was dried at 60 °C for 24 h.

In the final stage, 0.30 g of ND@FA mixture was mixed with 25 mL of EtOH and dispersed for 30 min. Then, 0.9 mmol of copper(II) nitrate (Cu(NO$_3$)$_2$·3H$_2$O) was added to the resulting suspension and refluxed for 24 h. The desired solution was centrifuged for 10 min at 4000 rpm to separate the precipitate, and after washing with ethanol 3 times, it was dried at room temperature for 24 h (Scheme 1a).

2.3. General procedure for the synthesis of tetrazole derivatives

In a flask, a mixture of benzaldehyde derivative (1 mmol), malononitrile (1 mmol), sodium azide (1.2 mmol), and 30 mg of catalyst (ND@FA-Cu(II)) in EtOH (10 mL) were stirred at 80 °C for 4 h. The completion of the reaction was monitored by thin-layer chromatography (TLC). After the reaction was complete, 10 mL of hydrochloric acid (2 M) was added to the reaction mixture with vigorous stirring. The catalyst was then easily separated by filtration. Subsequently, 20 mL of ethyl acetate was added to the reaction mixture and the organic and aqueous phases were separated using a separating funnel. Then, the catalyst was easily separated by filtration. The pure product obtained from the reaction mixture was recrystallized from hot ethanol (Scheme 1b). All the products were known compounds identified by characterization of their melting points (as indicated in Table 3) through comparison with authentic literature samples and, in some cases, their FT-IR and ^{1}H NMR spectral data.

2.4. General procedure for the synthesis of tetrazole derivatives from benzyl alcohols

In a flask, a mixture of benzyl alcohol derivatives (1 mmol), 2 mmol of tert-butyl hydroperoxide (TBHP), malononitrile (1 mmol), sodium azide (1.2 mmol), and 30 mg of catalyst (ND@FA-Cu(II)) in EtOH (10 mL) were stirred at 70 °C for 4 h. The completion of the reaction was monitored by thin-layer chromatography (TLC). After the reaction, 10 mL of 2 M hydrochloric acid was added to the reaction mixture with vigorous stirring. The catalyst was then easily separated by filtration. Next, 20 mL of ethyl acetate was added to the reaction mixture and the organic and aqueous phases were separated using a separating funnel. Then, the catalyst was easily separated by filtration.
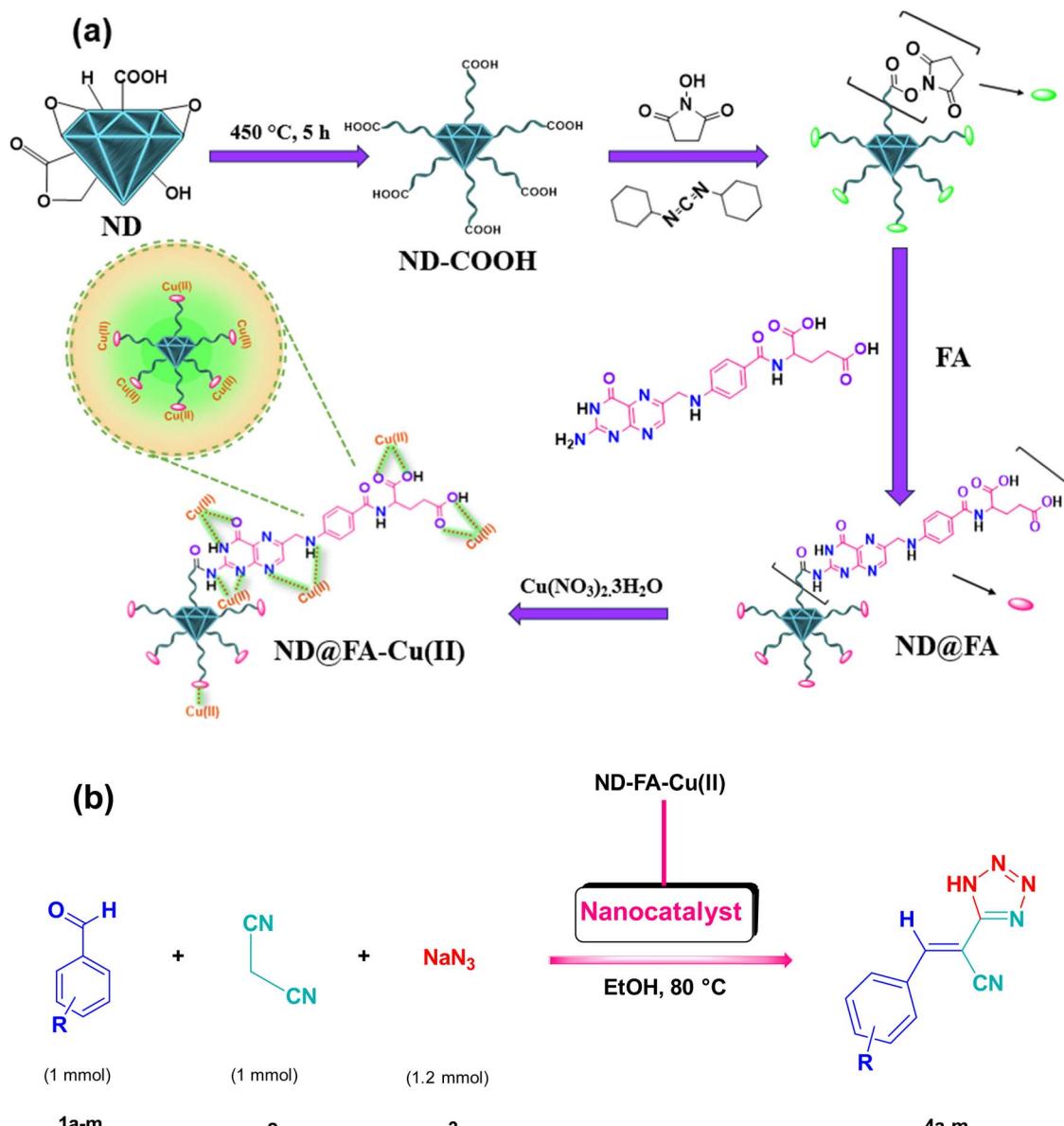
Scheme 1 Preparation of ND@FA-Cu(II) nanocatalyst (a), synthesis of tetrazole derivatives in the presence of ND@FA-Cu(II) (b).

The pure product obtained from the reaction mixture was recrystallized from hot ethanol. All the products were known compounds identified by characterization of their melting points (as indicated in Table 3) through comparison with authentic literature samples and, in some cases, their FT-IR and ^{1}H NMR spectral data.

2.5. Spectroscopic data for methyl (E)-4-(2-cyano-2-(1H-tetrazol-5-yl(vinyl)benzoate (4d)

White solid, M.p. 195–197 °C; IR (KBr, ν, cm^{-1}): 3452, 3100, 2910, 2394, 2184, 1636, 1512, 1344, 1238. ^{1}H NMR (500 MHz, DMSO): δ_H (ppm) = 2.5 (s, 1H, N–H over lab with DMSO), 3.89 (s, 3H, C–H), 8.10–8.13 (m, 4H, ArH), 8.53 (s, 1H, C–H). ^{13}C NMR (125 MHz, DMSO): δ_C (ppm) = 52.96, 99.68, 115.39, 116.30, 130.09, 130.11, 132.225, 136.43, 146.77, 166.09.

3 Results and discussion

3.1. Characterization of ND@FA-Cu(II) nanocatalyst

To comprehensively characterize the ND@FA-Cu(II) nanocatalyst and validate its structural, thermal, and elemental properties, a suite of complementary instrumental techniques was utilized. Fourier Transform Infrared (FT-IR) spectroscopy (Tensor 27, Bruker, Germany) was applied to confirm the successful surface modification of nanodiamonds, their covalent bonding with folic acid, and the effective formation of the final nanocatalyst. X-ray Diffraction (XRD) analysis (Bruker D8 Advance, Germany) was used to examine the crystalline structure of the catalyst and confirm its phase purity and structural stability throughout synthesis. Field Emission Scanning Electron Microscopy (FE-SEM, Sigma-Zeiss 300, Germany) was

employed to analyze the morphology and particle size distribution of the catalyst, while Energy Dispersive X-ray Spectroscopy (EDS, Numerix DXP-X10P model) was used to determine the elemental composition and quantify the amount of copper loaded onto the surface of the nanocatalyst. Thermogravimetric Analysis (TGA, Bahr STA 504, Germany) was conducted to evaluate the thermal stability of the catalyst, quantify its organic/inorganic content, and assess the efficiency of component loading during synthesis. ^1H and ^{13}C Nuclear Magnetic Resonance (NMR) spectra were recorded using a Varian-Inova 500 MHz spectrometer (USA) to confirm the chemical structure of the tetrazole derivatives synthesized in the catalytic process.

The FT-IR spectrum of the ND@FA-Cu(II) nanocatalyst is shown in Fig. 1. As indicated in Fig. 1a, the absorption band at 1708 cm^{-1}, shows the stretching vibration of the carbonyl bond (C=O) in the oxidized ND structure. The appearance of bands at 2918 and 2848 cm^{-1} was assigned to the asymmetric and symmetric C–H stretching vibrations. Additionally, the prominent peak at 3424 cm^{-1} describes the asymmetric stretching vibration of the O–H groups.[28,29] These interpretations explain the carboxylation of nanodiamonds. Fig. 1b and c display the FT-IR spectrum of the final stage of ND@FA-Cu(II) nanocatalyst synthesis. The strong peak at 1777 cm^{-1} indicates the stretching mode of the carbonyl ester group (C=O).[30] The absorption bands in the region of 2922 and 3221 cm^{-1} are associated with
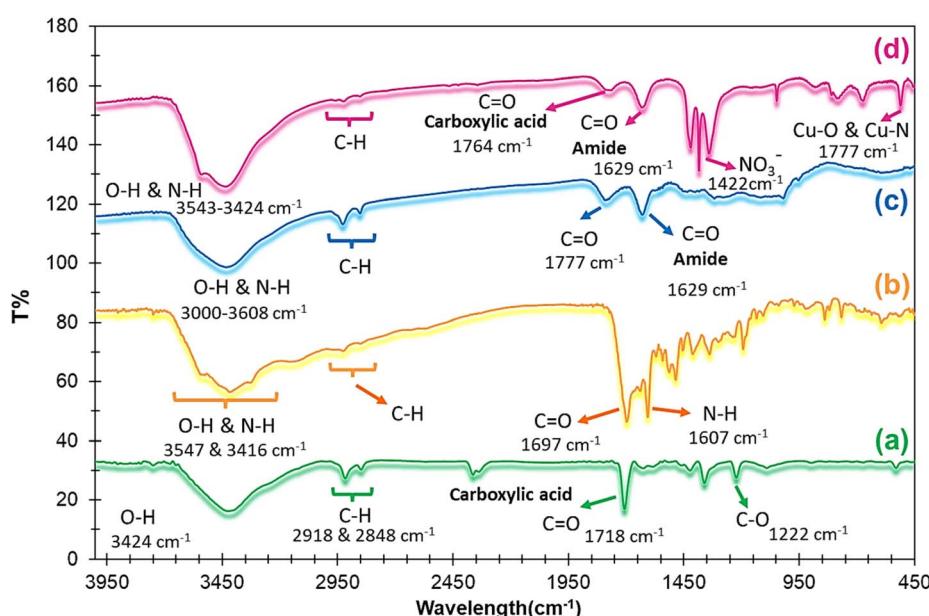

Fig. 1 FT-IR spectrum of ND-COOH (a), FA (b), ND@FA (c), and ND@FA-Cu(II) nanocatalyst (d).
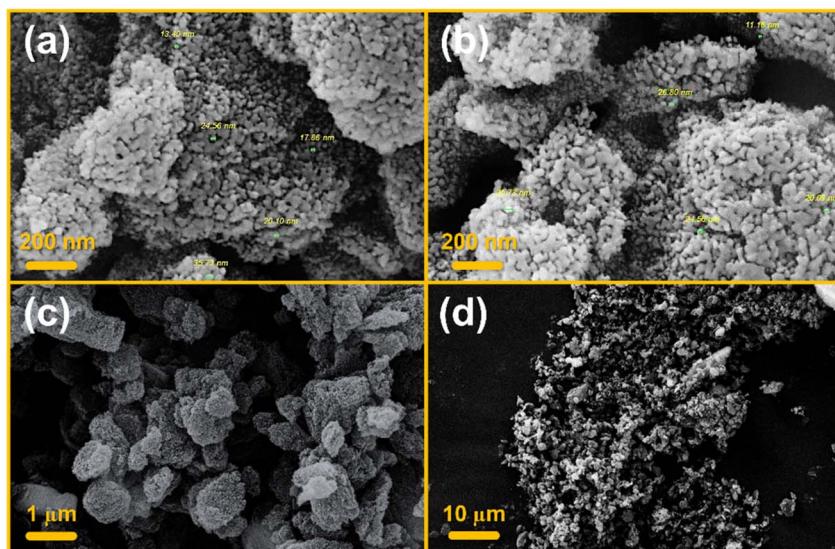

Fig. 2 FE-SEM images of ND@FA-Cu(II) nanocatalyst (a–d).

the symmetric and asymmetric stretching vibration of the C–H bond. The strong peak that appears at 3420 cm^{-1} represents the asymmetric stretching modes of the N–H and O–H groups. Additionally, the peak at 1629 cm^{-1} corresponds to the amide group (C=O), which explains the interaction between folic acid and nanodiamonds.

In Fig. 2a–d, the morphology and distribution of the ND@FA-Cu(II) nanocatalyst are analyzed using FE-SEM images at different magnifications. Fig. 2a and b are taken at a size of 200 nm from different angles, and Fig. 2c and d are seen at sizes of 1 μm and 10 μm, respectively. The particle size in the range of 10 to 40 nm in Fig. 2a and b indicates the formation of nano-sized particles. In addition, the folic acid coating increases the particle size. The images show that the diamond nano-particles are spherical, relatively uniform, and regularly distributed on the surface. However, it is observed here that the nanodiamond nanoparticles coated with folic acid effectively prevent interaction with each other and the effects of ultrasonic waves also prevent agglomeration. Also, due to the presence of single particles at all points of the coating, a proper distribution of nanoparticles is observed.

The EDS spectrum and mapping analysis of the ND@FA-Cu(II) nanocatalyst were illustrated in Fig. 3a. The presence of a C with an abundance of (68.83%) is due to the presence of nanodiamonds in the composition. Also, the N (16.17%) is related to folic acid. The O element is also (13.38%), and the presence of Cu in this analysis (1.62%) indicates the successful formation of the desired nanocatalyst. Mapping images show the uniform and dispersed distribution of elements in the ND@FA-Cu(II) nanocatalyst (Fig. 3b–3e).

The XRD diffraction patterns of ND@FA-Cu(II) nanocatalyst were monitored in Fig. 4. The characteristic peaks at $2\theta = 21.89°$ and 43.4° are related to oxidized ND structure (JCPDS card No: 96-110-0920).[31] The characteristic peaks at $2\theta = 12.7°$ and 25.8° are related to the crystalline phase of FA, which corresponds to the diffraction pattern of free folic acid (JCPDS card No: 96-222-0898),[32] and the peaks at $2\theta = 33.55°$ and 36.37° were attributed to copper (JCPDS card No: 96-900-9158).[33,34]

TGA analysis provided valuable insights into the thermal behavior, component composition, and loading efficiency of the nanocatalyst. It allowed for the estimation of the relative weight percentages of surface-bound folic acid, organic linkers, and residual copper content. By monitoring weight loss patterns across defined thermal regions, the thermal stability of the catalyst and the decomposition temperatures of both organic and inorganic moieties were identified. Within the temperature range of 50 to 200 °C, the observed weight loss of 17.3% stems from organic solvent evaporation and water molecule removal, typically associated with moisture and solvent evaporation in the sample. Subsequently, between 200 and 420 °C, a 10.64% weight loss occurs due to the decomposition of FA organic compounds. Moving forward, from 420 to 800 °C, a 31.78% weight loss is attributed to the decomposition of the ND scaffold. Additionally, the remaining portion (48.86%) correlates with the unaltered metal and the ND, which exhibit no decomposition due to their inherent nature and high thermal stability (Fig. 5).[35] The comparison of thermal profiles before and after surface functionalization confirmed the successful covalent attachment of FA and effective loading of Cu(II) onto the ND surface, indicating the successful synthesis of the catalyst.

3.2. Catalytic application of ND@FA-Cu(II) nanocatalyst in the synthesis of tetrazole derivatives

Initially, we optimized the catalytic efficiency of different catalysts such as ND, ND-COOH, ND@FA, ND@FA-Cu(II) (Table 1, entries 2–5) applied for a one-pot multicomponent reaction of 4chlorobenzaldehyde (1 mmol), malononitrile (1 mmol), and sodium azide (1.2 mmol) in EtOH at 80 °C as a model reaction. Next, the impact of temperature on the reaction efficiency was investigated (Table 1, entries 12–13). It was observed that when the reaction was complete at room temperature, we obtained 20% yields. As the temperature increased, the reaction yield also increased. Following that, we studied the effects of various solvents in the tetrazole synthesis (entries 9–11). Based on the results obtained from Table 1, the best solvent for achieving the
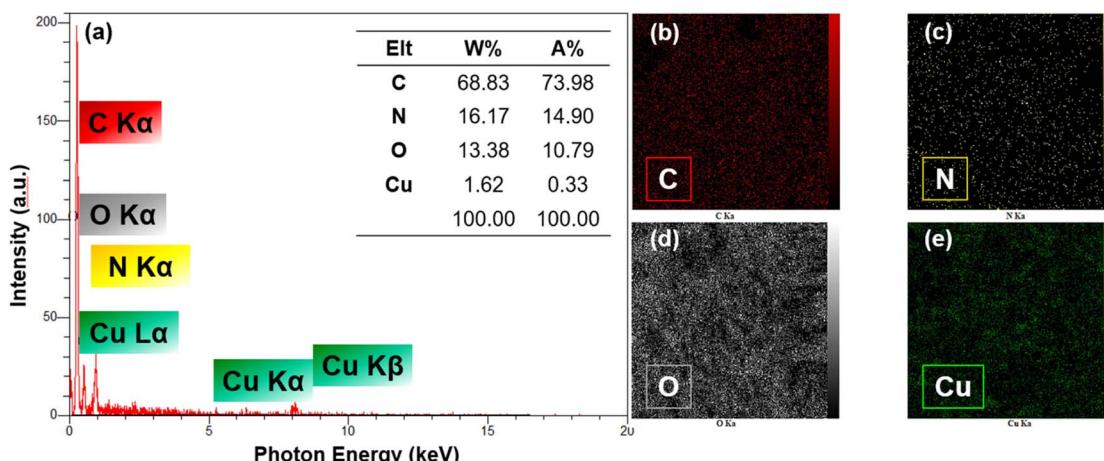

Fig. 3 EDS analysis (a) and mapping analysis (b−e) of ND@FA-Cu(II) nanocatalyst.

© 2025 The Author(s). Published by the Royal Society of Chemistry
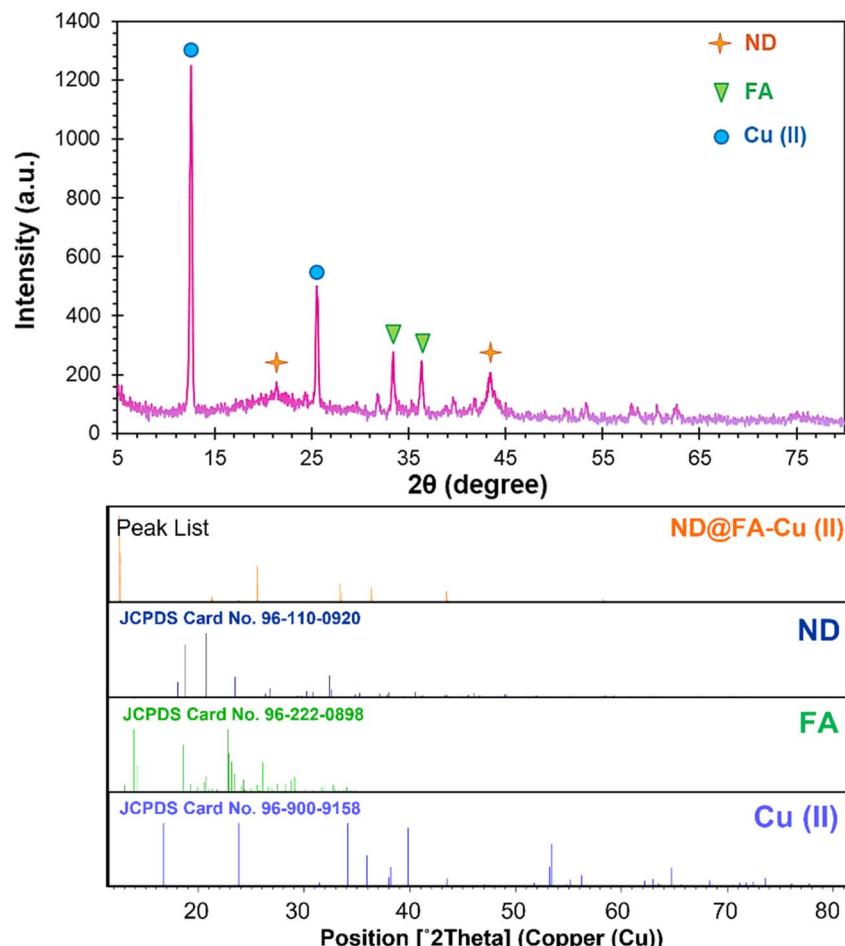
Fig. 4 XRD patterns of ND@FA-Cu(II) nanocatalyst.
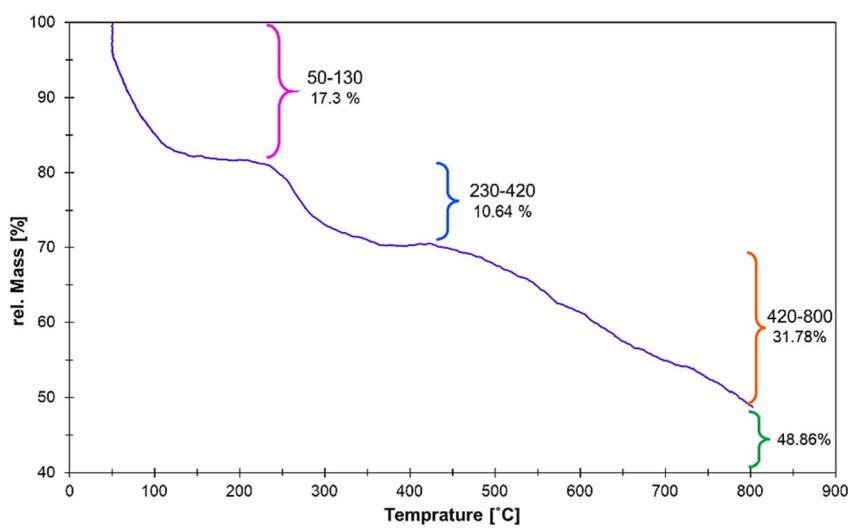
Fig. 5 TGA analysis of ND@FA-Cu(II) nanocatalyst.

highest yields in the reaction is EtOH green solvent. Finally, we examined the effects of catalyst dosage in the tetrazole synthesis (entries 6–8) and found that using 30 mg of ND@FA-Cu(II) nanocatalyst to complete the reaction after 4 h resulted in a 97% yield in 10 mL of EtOH, which is sufficient as a green solvent under reflux conditions.

Table 1 Optimization of the reaction conditions in the synthesis of tetrazole derivatives

Entry	Catalyst	Catalyst amount (mg)	Solvent	Temp (°C)	Time (h)	Yield
1	—	10	EtOH	Reflux	24	35
2	ND	10	EtOH	Reflux	4	45
3	ND-COOH	30	EtOH	Reflux	4	62
4	ND@FA	30	EtOH	Reflux	4	78
5	ND@FA-Cu(II)	30	EtOH	Reflux	4	97
6	ND@FA-Cu(II)	10	EtOH	Reflux	4	87
7	ND@FA-Cu(II)	20	EtOH	Reflux	4	94
8	ND@FA-Cu(II)	40	EtOH	Reflux	4	97
9	ND@FA-Cu(II)	30	H_2O	Reflux	4	78
10	ND@FA-Cu(II)	30	DMF	110	4	81
11	ND@FA-Cu(II)	30	CH_2Cl_2	35	4	54
12	ND@FA-Cu(II)	30	EtOH	r.t	4	20
13	ND@FA-Cu(II)	30	EtOH	50	4	85

Table 2 presents a comparison between the present work and earlier reports on the synthesis of **4c**. Based on the comparative data presented in this table, the ND@FA-Cu(II) nanocatalyst exhibits outstanding catalytic performance in terms of reaction yield, duration, solvent selection, and operational conditions relative to previously reported systems. The most remarkable advantage of this catalyst is its exceptionally high yield (97%) within just 4 h, whereas many prior systems required extended reaction times ranging from 8 to 24 h to achieve lower yields (typically 35–70%). This demonstrates the superior catalytic activity and optimized efficiency of the Cu(II) active sites uniformly distributed on the nanodiamond surface. Furthermore, the use of ethanol as a green, safe, and inexpensive solvent represents a critical environmental and economic advantage over many previously reported methods that rely on toxic, volatile, or non-ecofriendly solvents such as DMF or acetonitrile. The current transformation proceeds efficiently under mild reflux conditions, in contrast to other approaches that necessitate elevated temperatures. The innovative structural design of the ND@FA-Cu(II) nanocatalyst featuring the targeted coordination of Cu(II) ions onto folic acid-functionalized nanodiamonds enables excellent thermal and chemical stability, uniform dispersion of active metal sites, and reproducible catalytic behavior upon recycling. These features are well supported by structural analyses (XRD, FE-SEM, and EDS) and recycling studies, which confirmed sustained catalytic

performance over five consecutive cycles. Collectively, these attributes render ND@FA-Cu(II) a novel, green, cost-effective, and industrially viable catalytic system for efficient oxidative transformations under sustainable conditions.

After optimizing the reaction conditions, in order to check the scope and generality of these conditions' synthesis of a various of tetrazole derivatives was studied under reaction conditions. Table 3 shows that all the products were obtained in excellent yield after the appropriate reaction time.

To assess the catalytic efficiency in oxidation reactions, benzyl alcohols served as precursors for producing benzaldehydes in the tetrazole synthesis reaction. Initially, the catalyst, in conjunction with the oxidizing agent (TBHP), facilitated the oxidation of benzyl alcohols to benzaldehyde derivatives. Subsequently, in the reaction process involving sodium azide and malononitrile, tetrazole derivatives were synthesized.

To examine the scope and generality of these reaction conditions, the synthesis of various tetrazole derivatives was investigated. Table 4 illustrates that all products were obtained with excellent yield following the respective reactions.

The catalytically active sites of the ND@FA-Cu(II) nanocatalyst can be categorized into two main classes, both of which synergistically contribute to the efficiency of the oxidation reactions:

The Cu(II) sites are complexed with folic acid moieties and stabilized on the nanodiamond surface *via* carboxylic and

Table 2 Comparison of some catalysts' effects with ND@FA-Cu(II) nanocatalyst on the model reaction

Entry	Catalyst	Solvent	Temp (°C)	Time (h)	Yield	Ref.
1	ND@FA-Cu(II)	EtOH	Reflux	4	97	This work
2	Fe_3O_4@fibroin-SO_3H	EtOH	Reflux	40 min	45	36
3	Fe_3O_4@SiO_2	EtOH	Reflux	5	35	37
4	OPNSA	—	100	10	80	38
5	Nano-NiO	DMF	70	6	90	39
6	[BMIM]N_3	Acetonitrile	Reflux	24	39	40
7	NH-Cu(II)@MNP	EtOH	Reflux	10	91	41
8	Fe_3O_4@BNPs-CPTMS-Chitosan-Pd(0)	H_2O	80	1	40	42
9	Fe_3O_4-CNT-SO_3H	H_2O	80	2.5	45	43

Table 3 Synthesis of tetrazole derivatives with ND@FA-Cu(ɪɪ) nanocatalyst
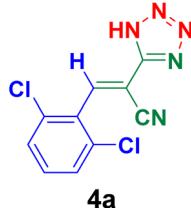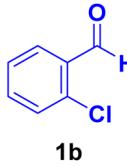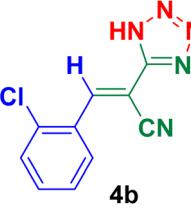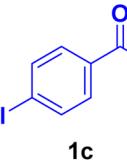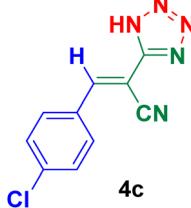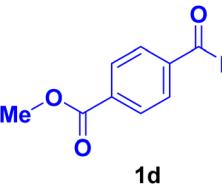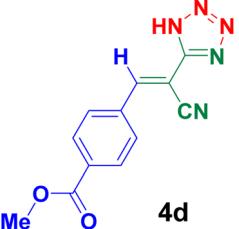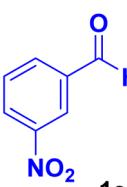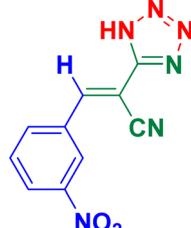
Entry	Aldehyde (1a–m)	Product (4a–m)	Time (h)	Yield (%)	Mp (°C) Observed	Mp (°C) Literature
1	1a	4a	4	92	189–192	New
2	1b	4b	4	94	173–175	175–177 (ref. 44)
3	1c	4c	4	97	162–165	164–166 (ref. 27)
4	1d	4d	4	95	195–197	New
5	1e	4e	4	91	160–162	161–163 (ref. 27)

Table 3 (*Contd.*)
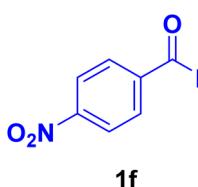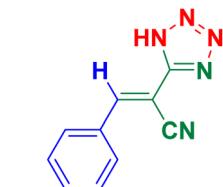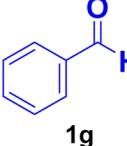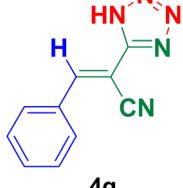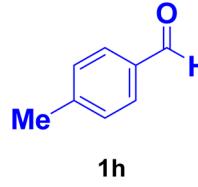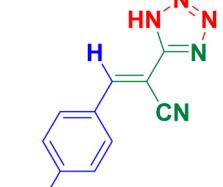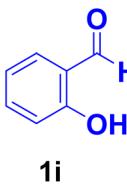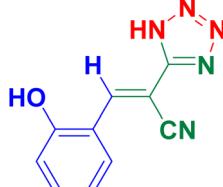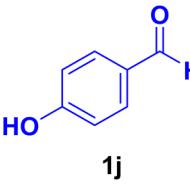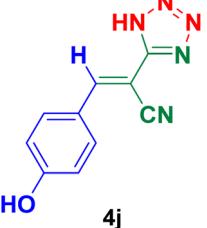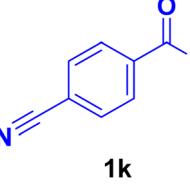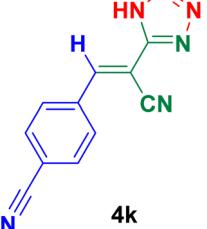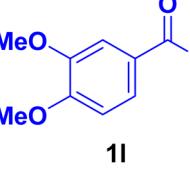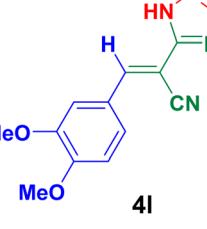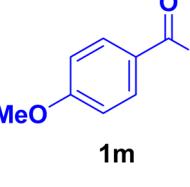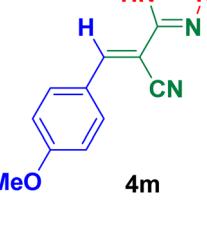
Entry	Aldehyde (**1a–m**)	Product (**4a–m**)	Time (h)	Yield (%)	Mp (°C) Observed	Literature
6	**1f**	**4f**	4	93	163–165	166–168 (ref. 43)
7	**1g**	**4g**	4	90	171–172	168–170 (ref. 45, 49)
8	**1h**	**4h**	4	89	193–195	190–192 (ref. 27, 50)
9	**1i**	**4i**	4	83	170–173	New

Table 3 (*Contd.*)

Entry	Aldehyde (**1a–m**)	Product (**4a–m**)	Time (h)	Yield (%)	Mp (°C) Observed	Literature
10	**1j**	**4j**	4	87	160–162	160–162 (ref. 27)
11	**1k**	**4k**	4	92	192–194	New
12	**1l**	**4l**	4	83	193–195	190–192 (ref. 46)
13	**1m**	**4m**	4	90	153–155	154–157 (ref. 47)

amide functional groups. In Scheme 2a, Cu(II) ions act as the primary redox-active centers and are responsible for the activation of the oxidant tert-butyl hydroperoxide (TBHP). During the reaction, Cu(II) facilitates the oxidation of benzyl alcohols to aldehydes, often *via* radical or non-radical mediators. The catalytic activity of Cu(II)-based systems in oxidation reactions

Table 4 Synthesis of tetrazole derivatives with ND@FA-Cu(ɪɪ) nanocatalyst from benzyl alcohols

| Entry	Aldehyde (**1a–m**)	Product (**4a–m**)	Time (h)	Yield (%)	Mp (°C)	
					Observed	Literature
1	**2n**	**4n**	6	95	167–170	164–166 (ref. 27)
2	**2o**	**4o**	6	86	158–160	161–163 (ref. 27)
3	**2p**	**4p**	6	90	165–167	168–170 (ref. 45)
4	**2q**	**4q**	6	87	157–159	160–161 (ref. 27)

involving TBHP as an oxidant has been widely documented, and numerous studies support the radical-mediated mechanism. For example, a Cu(ɪɪ) Schiff base complex embedded in a layered double hydroxide (LDH) showed efficient selective oxidation of ethylbenzene *via* activation of TBHP, where the absence of catalyst or TBHP suppressed the reaction, indicating the critical role of Cu(ɪɪ) centers in radical generation and substrate oxidation.[48] Similarly, the oxidation of ethylbenzene using
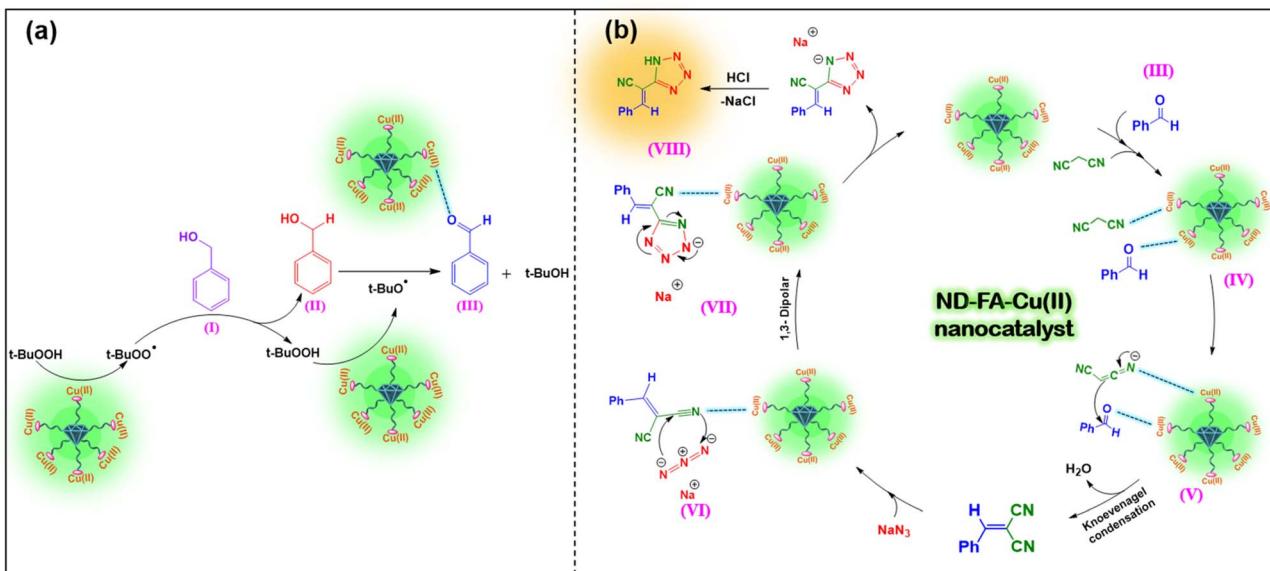
Scheme 2 One-pot oxidation of benzyl alcohol (a), the proposed reaction mechanism for the synthesis of tetrazole derivatives (b), catalyzed by ND@FA-Cu(II) nanocatalyst.

macrocyclic tri and tetra-aza copper complexes encapsulated in zeolite-Y showed that Cu(II) sites facilitate the formation of tert-butoxyl and benzyl radicals from TBHP and drive the selective oxidation process.[49] Furthermore, hydrotalcite-supported Cu–Al catalysts efficiently catalyze the oxidation of benzyl alcohols to carbonyl compounds by a mechanism involving surface peroxide intermediates and radicals generated through Cu(II)-mediated activation of TBHP.[50]

Taken together, these studies strongly support that the ND@FA-Cu(II) nanocatalyst likely follows a similar radical initiation and propagation mechanism during benzyl alcohol oxidation, such that the Cu(II) centers activate TBHP to generate reactive radical species essential for the oxidation process. On the other hand, the surface oxygenated functional groups on ND@FA include –COOH, –OH, and –CONH– groups, which not only enhance the dispersion of Cu(II) species on the surface, but also provide a hydrophilic and chemically stable environment for the stabilization of intermediate species and transition states. These functional groups improve the solid–liquid interfacial interactions and facilitate efficient electron transfer during the catalytic cycle. The integration of redox-active Cu(II) centers with good dispersion and a surface architecture rich in polar functional groups results in a highly efficient and recyclable nanocatalyst. This two-site catalytic platform offers significant advantages in terms of activity, selectivity, and reusability, introducing ND@FA-Cu(II) as a promising heterogeneous system for green oxidation processes.

The proposed mechanism for synthesizing 1H-tetrazole derivatives using ND@FA-Cu(II) nanocatalyst in Scheme 2b. Initially, benzaldehyde and malononitrile's oxygen and nitrogen atoms interact via lone pairs of electrons with active sites on the surface of the catalyst. In this way, the carbonyl group in benzaldehyde and the cyano group in malononitrile are activated through interaction with Cu(II). In the next step,

the carbon of the C≡N group, as a nucleophile, attacks the carbonyl group of benzaldehyde (III), and through the Knoevenagel reaction, a carbon–carbon double bond is formed (V). Then, the negatively charged nitrogen in the sodium azide compound attacks the intermediate cyano group (VI). Finally, the 5-membered ring is formed by 1,3-dipolar cycloaddition as product (VII). After the completed reaction, the nanocatalyst is re-formed from compound (VII) and exits the reaction cycle. Finally, tetrazole is formed as the final product (VIII).

3.3. Recyclability of ND@FA-Cu(II) nanocatalyst

The recyclability of the catalyst is one of the most important advantages and makes it useful for commercial applications. For this reason, ND@FA-Cu(II) nanocatalyst was used several times in the production process of tetrazole derivatives. After the completion of the reaction, the nanocatalyst was filtered and washed several times with diethyl ether, dried, and reused in subsequent reactions. Each recycling experiment was independently repeated three times under identical conditions. In Table 5, the results are expressed as mean ± standard deviation (SD), and the corresponding error bars are provided in Fig. 6a. The standard deviation values ranged from ±1.25 to ±2.08,

Table 5 Recyclability of the catalyst: yields, mean, and standard deviation over five cycles

| Recycling cycle	Run 1 [yield (%)]	Run 2 [yield (%)]	Run 3 [yield (%)]	Mean ± SD
1st	95	96	98	96.3 ± 1.25
2nd	92	94	96	94.0 ± 2.00
3rd	89	91	92	90.7 ± 1.53
4th	87	88	91	88.7 ± 2.08
5th	84	86	88	86.0 ± 2.00
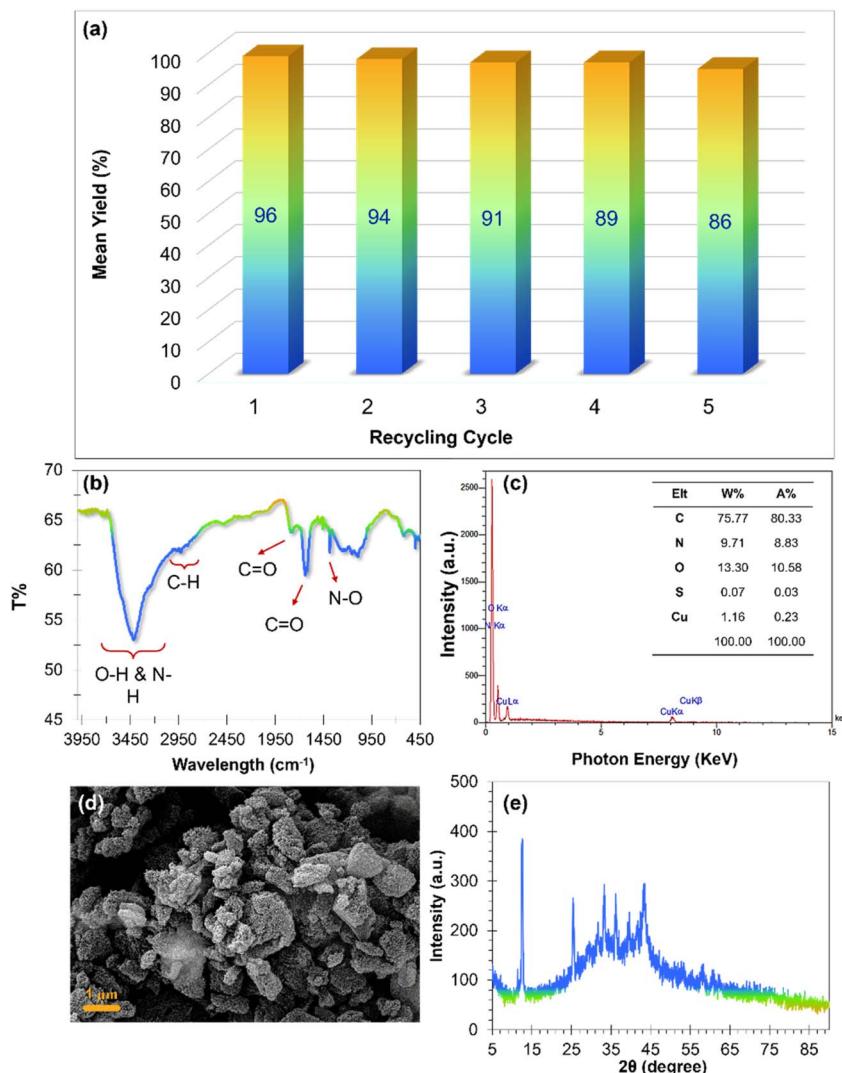
Fig. 6 Reusability diagram (a), FT–IR spectrum (b), EDS analysis (c), FE–SEM image (d), and XRD pattern (e) of recycled ND@FA-Cu(ɪɪ) nanocatalyst.

indicating acceptable reproducibility and catalytic performance across all cycles. This consistency confirms the structural and functional stability of the catalyst under oxidative conditions. To evaluate the structural stability of the ND@FA-Cu(ɪɪ) nanocatalyst under oxidative reaction conditions, FT-IR, EDS, FE-SEM images, and XRD patterns were analyzed before and after the catalytic process. First, by examining the FT-IR spectrum of the recycled catalyst, it can be seen that the structure of the nanocatalyst was still maintained after the oxidation reaction (Fig. 6b). EDS analysis also showed that the catalyst elements are still intact after recycling (Fig. 6c). FE-SEM results showed that the overall morphology, particle size, and surface homogeneity of the nanocatalyst remained virtually unchanged after the reaction. No signs of particle aggregation, surface collapse, or structural degradation were observed, confirming the strong structural integrity of the catalyst under thermal and chemical stress (Fig. 6d).

Furthermore, comparison of the XRD patterns before and after the oxidation reaction showed no significant changes or shifts in the positions and intensities of the diffraction peaks

(Fig. 6e). The characteristic reflections corresponding to the ND, FA, and Cu(ɪɪ) species remained constant, indicating that both the crystal structure and the copper-based active phase were preserved during the reaction. Collectively, these observations confirm the high crystallographic and structural stability of the ND@FA-Cu(ɪɪ) catalyst, which, together with its excellent recyclability, highlights its suitability for stable and repeated oxidative transformations.

4   Conclusion

In summary, the fabrication of the novel ND@FA-Cu(ɪɪ) nanocatalyst *via* the functionalization of nanodiamond with folic acid has been successfully achieved. Characterization techniques including FT-IR, EDS, XRD, FE-SEM, and TGA have confirmed the formation and properties of the nanocatalyst. The catalytic performance of ND@FA-Cu(ɪɪ) nanocatalyst in the synthesis of tetrazole derivatives has been investigated, demonstrating excellent efficiency, low reaction time, and mild conditions. The synthesized products were characterized using

FT-IR, ^{1}HNMR, ^{13}C NMR, and melting point analysis. Notably, the nanocatalyst exhibited high yields (83–97%) in the synthesis of 1H-tetrazole derivatives with various substituents, showcasing its versatility and efficiency. Furthermore, the ability of the nanocatalyst to be reused up to 5 times without significant loss of catalytic activity highlights its economic and environmental advantages. The prepared nanocomposite has also shown promising performance in Knoevenagel condensation and [2 + 3] cycloaddition reactions, further demonstrating its versatility in organic synthesis. Overall, the design, fabrication, and characterization of ND@FA-Cu(II) nanocomposite, along with its exceptional catalytic properties in various organic reactions, signify a significant advancement in the field of green chemistry. This study paves the way for the development of efficient and sustainable catalytic systems for organic synthesis, contributing to the promotion of environmentally friendly chemical processes. Additionally, the utilization of benzyl alcohol precursors in the synthesis of tetrazole derivatives in a one-pot reaction further underscores the versatility and efficiency of this catalyst. In oxidation reactions, ND@FA-Cu(II) nanocatalyst demonstrates excellent performance as a catalyst under green chemistry conditions, highlighting its potential for environmentally friendly chemical processes.

Author contributions

Arezoo Ramezani: methodology, experimental, data analysis, investigation, writing – original draft, review and editing. Reza Ghalavand: writing – original draft. Zahra Nasri: writing – original draft, review and editing. Hossein Ghafuri: supervision, providing instrumental facilities.

Conflicts of interest

The authors declare that they have no known competing financial interests or personal relationships that could have appeared to influence the work reported in this paper.

Data availability

All data supporting the findings of this paper are available within the manuscript and its SI file. Additional supporting information including spectroscopic characterization data of the nanocatalyst and the products such as FT-IR and[18,28] ^{1}H NMR can be found in the online version of this article at the publisher's website. See DOI: **https://doi.org/10.1039/d5ra03496e**.

Acknowledgements

References

1 M. S. Ali, et al., Int. J. Pharm., 2019, **558**, 165–176.

2 P. Gao, et al., Nat. Commun., 2021, **12**(1), 4698.

3 Y. Pan, et al., Appl. Catal., B, 2020, **265**, 118579.

4 A. J. Brachtenbach, Characterization of MSY Nanodiamonds as a Nanoparticulate Adjuvant for RiVax Vaccine, University of Kansas, 2019.

5 Z. Qin, et al., Nat. Commun., 2023, **14**(1), 6278.

6 V. N. Mochalin, et al., Diam. Relat. Mater., 2015, **58**, 161–171.

7 A. Krueger, J. Mater. Chem., 2008, **18**(13), 1485–1492.

8 Z. Li, et al., Nat. Mater., 2023, **22**(1), 42–49.

9 P. Yan, et al., Nat.Commun., 2024, **15**(1), 9812.

10 F. Huang, et al., Nat. Commun., 2019, **10**(1), 4431.

11 N. Gupta, et al., Chem Cat Chem., 2016, **8**(5), 922–928.

12 G. Reina, et al., Angew. Chem., Int. Ed., 2019, **58**(50), 17918–17929.

13 S. Molaei and M. Ghadermazi, Sci. Rep., 2025, **15**(1), 16175.

14 S. Momeni, et al., Inorg. Chem. Commun., 2025, **178**, 114419.

15 X. Y. Wong, et al., Sci. Rep., 2021, **11**(1), 2375.

16 J. Acosta-Elia, et al., Front. Pharmacol., 2020, **11**, 1062.

17 S. Bagheri, et al., ChemistrySelect, 2019, **4**(40), 11930–11935.

18 M. Ahmad, et al., Food Hydrocoll., 2017, **66**, 154–160.

19 R. Matias, et al., J. Anal. Methods Chem., 2014, **6**(9), 3065–3071.

20 B. Stella, J. Pharma, et al., J. Pharmaceut. Sci., 2000, **89**(11), 1452–1464.

21 B. Maleki, et al., Polycycl. Aromat. Compd., 2024, **44**(2), 994–1010.

22 M. Ara, et al., Colloid Interface Sci. Commun., 2023, **53**, 100704.

23 R. Vishwakarma, et al., Chemistry Select, 2022, **7**(29), e202200706.

24 R. Uppadhayay, A. Kumar, J. Teotia, et al., J. Org. Chem., 2022, **58**(12), 1801–1811.

25 I. S. de Jesus, et al., J. Org. Chem., 2024, **89**(19), 14279–14290.

26 P. Das, S. Ganguly, A. Rosenkranz, et al., Mater. Today Nano, 2023, **24**, 100428.

27 Z. Hajizadeh, et al., RSC Adv., 2020, **10**(44), 26467–26478.

28 Z. Nasri, et al., Chem. Proc., 2024, **16**(1), 86.

29 H. Girard, T. Petit, S. Perruchas, et al., Phys. Chem. Chem. Phys., 2011, **13**(24), 11517–11523.

30 S. Mallakpour, et al., J. Polym. Res., 2020, **27**(9), 259.

31 A. Lesani, et al., J. Biomed. Mater. Res., Part B, 2022, **110**(6), 1391–1399.

32 U. Ruman, et al., Nanomater., 2021, **11**(2), 497.

33 H. Ghafuri, et al., Sci. Rep., 2022, **12**(1), 4221.

34 C. Hu, et al., Mater. Res., 2017, **20**(2), 407–412.

35 M. Banisaid, et al., Int. J. Chem. Sci., 2018, **16**, 262.

36 A. Nouri Parouch, et al., Res. Chem. Intermed., 2020, **46**(7), 3295–3310.

37 X. Yuan, et al., RSC Adv., 2019, **9**(41), 23614–23621.

38 Z. N. Tisseh, et al., Tetrahedron, 2012, **68**(6), 1769–1773.

39 J. Safaei-Ghomi, et al., Chem. Heterocycl. Compd., 2015, **50**, 1567–1574.

40 S. Khaghaninejad, et al., Res. Chem. Intermed., 2016, **42**, 1593–1610.

41 F. Ek, et al., Tetrahedron, 2003, **59**(35), 6759–6769.

42 M. Khodamorady, et al., ChemistrySelect, 2019, **4**(28), 8183–8194.

43 P. Akbarzadeh, *et al.*, *J. Heterocycl. Chem.*, 2020, **57**(6), 2455–2465.

44 P. Akbarzadeh, *et al.*, *Res. Chem. Intermed.*, 2019, **45**, 1009–1024.

45 C. Behloul, *et al.*, *Synthesis*, 2018, **50**(17), 3430–3435.

46 A. El-Sewedy, *et al.*, *Sci. Rep.*, 2023, **13**(1), 17869.

47 J. Safaei-Ghomi, Z. fur, *et al.*, *Z. Naturforsch. B Chem. Sci.*, 2015, **70**(11), 819–828.

48 J. S. Kirar and S. Khare, *RSC Adv.*, 2018, **8**(34), 18814–18827.

49 T. Bennur, *et al.*, *J. Mol. Catal. A: Chem.*, 2004, **207**(2), 163–171.

50 J. Mobley, *et al.*, *RSC Adv.*, 2015, **5**(81), 65780–65797.